Rapid Communications

Majorana-induced DC Shapiro steps in topological Josephson junctions

Sang-Jun Choi [1,*] Alessio Calzona,[1] and Björn Trauzettel[1,2]

[1]*Institute for Theoretical Physics and Astrophysics, University of Würzburg, D-97074 Würzburg, Germany*
[2]*Würzburg-Dresden Cluster of Excellence ct.qmat, Germany*

The demonstration of the non-Abelian properties of Majorana bound states (MBSs) is a crucial step toward topological quantum computing. We theoretically investigate how the fusion of MBSs manifests itself in the current-voltage characteristics of a topological Josephson junction. The junction is assumed to be built on U-shaped quantum spin Hall edges and is supposed to host a Majorana qubit formed by four MBSs. Inter- and intraedge couplings among adjacent MBSs provide two orthogonal components of the rotation axes of the Majorana qubit. We show that the interplay of the dynamics of the superconductor phase difference and the Majorana qubit governs the Josephson effect. Strikingly, we identify sequential jumps of the voltage across the junction with increasing DC current bias without external AC driving. Its role in the formation of ordinary Shapiro steps is replaced by the intrinsic Rabi oscillations of the Majorana qubit. We coin this phenomenon *DC Shapiro steps*.

Majorana bound states (MBSs) are non-Abelian excitations supported by topological superconductors and represent the building blocks of topological quantum computation [1–5]. The non-Abelian exchange statistic of MBSs allows for the implementation of topological quantum gates processing quantum information in a topologically protected manner [6,7]. A key property of MBSs, which serves as an indirect demonstration of non-Abelian statistics, is their nontrivial fusion properties [2,8]. In general, the fusion of two MBSs produces an equal-weight superposition of even and odd fermion parity. This implies that MBSs feature a nontrivial quantum dimension greater than one.

In condensed matter physics, several platforms capable of hosting and manipulating MBSs have been investigated, including semiconducting quantum wires [9–14] and more recently second-order topological superconductors [15–23]. Among other platforms, topological Josephson junctions (TJJs) have proven to be promising theoretically and experimentally [24–29]. Importantly, single-electron tunneling into a pair of MBSs in a TJJ leads to the fractional Josephson effect [30–33], recently confirmed by experiments [34–38] with missing odd Shapiro steps. These results, together with other seminal experimental observations [11,12,14,39], have deeply strengthened the evidence for MBS. More recently, intriguing Josephson effects stemming from nonlinear dynamics of MBSs have been suggested as a way to visualize the particular dynamics of Majorana qubits [40,41]. In this Rapid Communication, we pursue an approach adopting the same phenomenological model but study it in a different regime. It turns out that this difference leads to the novel phenomenon of *DC Shapiro steps* described below.

We consider a TJJ hosting four MBSs defining a Majorana qubit (see Fig. 1). Importantly, we allow a single MBS to fuse with different partners; for instance, γ_2 can develop an intraedge coupling with γ_1 and/or an interedge coupling with γ_3. This leads to nontrivial dynamics of the Majorana qubit, whose interplay with the dynamics of the phase difference affects the Josephson effect. Remarkably, the Majorana dynamics lowers the critical current I_c^* of the junction. Moreover, when a DC current bias increases over I_c^*, it induces sequential steps of the voltage drop V across the junction.

We coin this phenomenon DC Shapiro steps to emphasize its relation to the known AC Shapiro steps. Both in conventional and topological Josephson junction, AC Shapiro steps appear (under certain conditions) if a DC current bias—in combination with an AC current component—is applied across the junction [42,43]. By contrast, the novel DC Shapiro steps emerge without any external periodic drive. The role of the AC driving is replaced by the intrinsic (Rabi) oscillations of the Majorana qubit, whose frequency can be estimated from the height of the steps. The importance of the novel DC Shapiro steps is twofold: (i) They represent a new phenomenon in the realm of the Josephson effect. (ii) They are a manifestation of the nontrivial fusion of MBSs.

Setup. We consider the TJJ sketched in Fig. 1, consisting of the edge of a quantum spin Hall (QSH) insulator which is proximitized by two superconductors separated by a ferromagnetic region [30]. The Hamiltonian of the system is $H = \frac{1}{2} \int dx\, \Psi^\dagger(x)\mathcal{H}(x)\Psi(x)$ with

$$\mathcal{H}(x) = \tau_z[-i\hbar v \partial_x s_z - \mu(x)] + \mathbf{M}(x) \cdot \mathbf{s}$$
$$+ \Delta_0(x)[\tau_x \cos\varphi + \tau_y \sin\varphi], \quad (1)$$

where $\Psi^\dagger(x) = [\psi_\uparrow^\dagger(x),\ \psi_\downarrow^\dagger(x),\ \psi_\downarrow(x),\ -\psi_\uparrow(x)]$, and $\psi_s^\dagger(x)$ and $\psi_s(x)$ are the creation and annihilation operators of electrons with spin index s. Pauli matrices $s_{x,y,z}$ and $\tau_{x,y,z}$
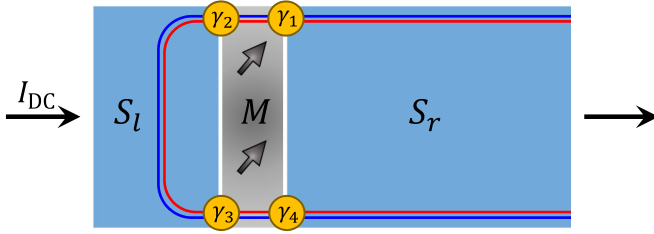
*sang-jun.choi@physik.uni-wuerzburg.de

FIG. 1. Josephson junction formed on U-shaped QSH edges hosting four MBS $\gamma_{1,2,3,4}$. Counterpropagating QSH edges are colored with blue and red lines. The region with in-plane magnetization **M** (gray) constitutes weak links between two superconductors S_l and S_r (blue). Pairs of two MBSs at the upper and lower sides of the junction compose two fermion parity states of $|0_{12}0_{34}\rangle$ and $|1_{12}1_{34}\rangle$. A superposition of them defines a Majorana qubit state $|Q\rangle$. Intraedge coupling provides the rotation of the Majorana qubit along the z axis, and interedge coupling along the x axis.

describe spin and particle-hole space, respectively; v is the Fermi velocity of QSH edge states. The chemical potentials in the region with magnetization and superconductors are, respectively, μ_M and μ_S. The superconducting phase difference of S_l and S_r is φ, and their proximity gap is $\Delta_0(x) = \Delta_0$. We assume a finite magnetization $\mathbf{M}(x) = \text{sgn}(x)(M\cos\phi, M\sin\phi, 0)$ only in the weak link between the superconductors. The distance between superconductors is L, and the length of the QSH edge in S_l is W. We consider that $\hbar v/W$ is much smaller than the bulk gap of the QSH insulator so that the upper and lower edges are completely decoupled in the other regions.

To characterize the junction, we consider at first the limits $\hbar v/L \ll M$ and $\hbar v/W \ll \Delta_0$, so that well-separated MBSs $\gamma_{i=1,2,3,4}$ appear at zero energy. Those are equal superpositions of spin-polarized electrons and holes $\gamma_i \propto \int dx[\psi_i^\dagger(x) + \psi_i(x)]$ localized at position x_i, where $\psi_i^\dagger(x) \propto e^{-|x-x_i|/\xi(x)}[\psi_\uparrow^\dagger(x) + e^{i\phi+i\theta_i(x)}\psi_\downarrow^\dagger(x)]$. The localization length $\xi(x)$ is inversely proportional to the size of the gap of the region at position x. Importantly, the spin polarization $\theta_i(x)$ is electrically tunable with chemical potentials: μ_M tunes θ_i at position x_i according to $\sin\theta_i(x_i) = (-1)^i\text{sgn}(x_i)\sqrt{1 - (\mu_M/M)^2}$; μ_S changes the length of the spin helix of γ_i in the superconducting regions, i.e., $\theta_i(x) = \theta_i(x_i) + 2(x - x_i)\mu_S/(\hbar v)$. In the M region, the spatial dependence of θ_i is $\theta_i(x) = \theta_i(x_i)$.

To enable the fusion of MBSs, we consider the following regime: $\hbar v/L \sim M$ and $\hbar v/W \sim \Delta_0$. Projecting the full Hamiltonian H on the Majorana wave functions, we obtain the effective low-energy Hamiltonian $H_{\text{eff}} = iE_x\gamma_2\gamma_3 + iE_z\gamma_1\gamma_2 + iE_z\gamma_3\gamma_4$. The interedge coupling through S_l is $E_x \propto \sin\{[\theta_2(x) - \theta_3(x)]/2\}$, where x is in S_l. E_x is vanishing (maximized) when the spin polarizations of γ_2 and γ_3 are (oppositely) aligned in the S_l region. Explicitly, the interedge coupling is

$$E_x = \frac{2\Delta_0\sqrt{M^2 - \mu_M^2}}{\Delta_0 + \sqrt{M^2 - \mu_M^2}}e^{-W\Delta_0/\hbar v}\sin\left(\frac{\mu_M}{M} + \frac{\mu_S W}{\hbar v}\right), \quad (2)$$

and the intraedge coupling reads $E_z = E_M\cos\frac{\varphi}{2}$. The derivation of Eq. (2) is provided in the Supplemental Material (SM) [44]. We stress that the magnetized region allows us to control the interedge coupling (via μ_M) and to get rid of other midgap states at higher energies.

In order to study the Josephson effect, we describe the junction in terms of the complex fermions $f_{ij} \equiv (\gamma_i + i\gamma_j)/2$, which mediate the supercurrent. In particular, Majorana fermions γ_1 and γ_2 define two oppositely current-carrying states coined $|0_{12}\rangle$ and $|1_{12}\rangle$. They satisfy $f_{12}|0_{12}\rangle = 0$ and $f_{12}^\dagger|0_{12}\rangle = |1_{12}\rangle$. Analogously, γ_3 and γ_4 provide current-carrying states $|0_{34}\rangle$ and $|1_{34}\rangle$. The total supercurrent across the junction is therefore controlled by the state of the Majorana qubit $|Q\rangle$. Importantly, states with total odd fermion parity do not carry any net supercurrent across the junction and they are invisible from a transport point of view [52]. By contrast, the generic state with even total fermion parity $|Q\rangle = \alpha|0_{12}0_{34}\rangle + \beta|1_{12}1_{34}\rangle$ carries a finite supercurrent $I_J = (|\alpha|^2 - |\beta|^2)\frac{eE_M}{\hbar}\sin\frac{\varphi}{2}$. In the following, we focus on the even-parity sector and recast H_{eff} in terms of the current-carrying fermion states, $H_{\text{eff}} = E_x\sigma_x + E_z\sigma_z$, where the basis is $\{|1_{12}1_{34}\rangle\}, |0_{12}0_{34}\rangle\}$. The off-diagonal elements E_x manifest as Rabi oscillations between the current-carrying two-level states of the Majorana qubit.

Josephson effect with Majorana dynamics. We consider an overdamped Josephson junction shunted by the normal resistor R_N. Under a DC current bias I_{DC}, the voltage drop $v(t)$ across the junction is described by the nonlinear differential equation [35,36,43]

$$I_{\text{DC}} = -\mathcal{Z}I_c\sin\frac{\varphi}{2} + \frac{\hbar}{2eR_N}\frac{d\varphi}{dt}, \quad (3)$$

where $\mathcal{Z} = \langle Q|\sigma_z|Q\rangle$ and $I_c = eE_M/\hbar$ in our setup. Dynamics of the phase $\varphi(t)$ is obtained by equating I_{DC} with the sum of the supercurrent I_J and the normal current $v(t)/R_N$, so that the voltage drop is determined by the Josephson relation $v(t) = \hbar/(2e)\dot\varphi(t)$. A mechanics analog provides complementary insight into the dynamics of $\varphi(t)$: Eq. (3) can be interpreted as the dynamics of a massless (phase) particle sliding along a tilted washboard potential $U(\varphi) = -I_{\text{DC}}\varphi + 2\mathcal{Z}I_c\cos\varphi/2$ [43].

Without interedge coupling, $E_x = 0$, $\mathcal{Z}$ is a conserved quantity: the profile of the associated washboard potential is fixed in time. In this case, a sudden change in $I_{\text{DC}} \leqslant I_c$ causes φ to evolve towards a fixed point φ_f satisfying $I_{\text{DC}} = -\mathcal{Z}I_c\sin\varphi_f/2$. During the transient regime, $\varphi(t)$ monotonically increases with a characteristic timescale $\tau_r = \hbar/(2eI_cR_N)$. Thus, a positive voltage $v(t)$ is temporarily generated and vanishes afterwards. For a larger DC current, $I_{\text{DC}} > I_c$, the phase φ increases with time and a finite average voltage drop across the junction is developed, $V = \lim_{\tau\to\infty}\frac{1}{\tau}\int_0^\tau v(t)dt$.

With a finite interedge coupling, $E_x > 0$, assumed to be positive without loss of generality, the behavior of the junction is controlled by the dynamics of both the phase particle and the Majorana qubit. To describe the latter, we introduce the unit vector $\mathbf{R} = (\mathcal{X}, \mathcal{Y}, \mathcal{Z})$ on the Bloch sphere, with $\mathcal{X} = \langle Q|\sigma_x|Q\rangle$ and $\mathcal{Y} = \langle Q|\sigma_y|Q\rangle$. Its dynamics is controlled by the
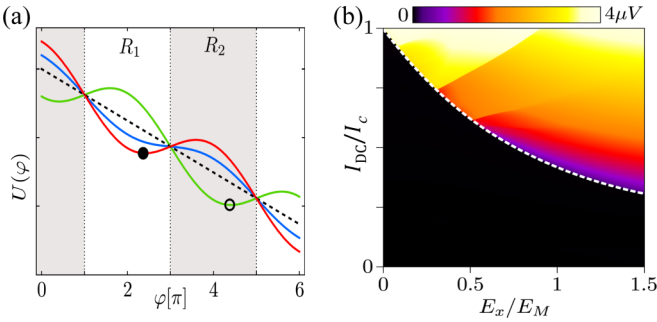
FIG. 2. (a) Sketch of the washboard potential $U(\varphi)$ when $\mathcal{Z} > \mathcal{Z}_{th}$ (red line), $0 < \mathcal{Z} < \mathcal{Z}_{th}$ (blue line), $\mathcal{Z} = 0$ (dashed line), and $\mathcal{Z} < -\mathcal{Z}_{th}$ (green line). When the Majorana qubit precesses with $\mathcal{Z} > 0$, the phase particle (solid circle) is recaptured in $\varphi \in R_1 = [\pi, 3\pi]$. After recapturing the phase particle by a certain number of times n, $\mathcal{Z}$ flips its sign, and the phase particle rolls down to $\varphi \in R_2 = [3\pi, 5\pi]$ (hollow circle). (b) Colormap of the time-averaged voltage V under DC current bias I_{DC} and the interedge coupling E_x. I_c^* in Eq. (5) is drawn as a guide for the eye (dotted line). V exhibits sequential jumps as increasing I_{DC}. We use $E_M = 5$ μeV and the experimental parameter of $2eI_cR_N/h \sim 2$ GHz extracted from Ref. [36].

equations of motion,

$$\frac{d\mathbf{R}}{dt} = \mathbf{N} \times \mathbf{R}, \tag{4}$$

where $\mathbf{N} = 2(E_x, 0, E_z)/\hbar$. $\mathbf{R}$ precesses around $\mathbf{N}$ with time period $\mathcal{T} = \pi\hbar/(E_x^2 + E_z^2)^{1/2}$ with time-independent E_z. However, as $E_z = E_M \cos\frac{\varphi(t)}{2}$, the precession axis $\mathbf{N}(t)$ changes according to Eq. (3), while the barrier height $\mathcal{Z}(t)$ in Eq. (3) changes simultaneously according to Eq. (4). The intertwined dynamics of the phase difference and Majorana qubit has been analyzed in Ref. [40] in terms of the Landau-Zener transition with an exponentially small parameter E_x/E_M. Contrarily, we focus on comparable parameters of E_x and E_M which is a crucial choice for the emergence of DC Shapiro steps.

To develop intuition about the interplay between the differential equations (3) and (4) with comparable E_x and E_M, we analyze the features of the washboard potential $U(\varphi)$. As shown in Fig. 2(a), for a DC current I_{DC}, the qubit state $\mathcal{Z}$ modulates the profile of $U(\varphi)$ with the constant overall slope in time due to the absence of AC driving. While $U(\varphi)$ is pinned at the points $\bar\varphi_j \equiv \pi \pmod{2\pi}$, as for the regions R_j, i.e., $\bar\varphi_{j-1} \leqslant \varphi < \bar\varphi_j$, in between those points, two configurations are possible: (i) If $|\mathcal{Z}|$ exceeds the threshold $\mathcal{Z}_{th} = I_{DC}/I_c$, the regions feature an alternating pattern of local minima and maxima [red and green lines in Fig. 2(a)]. (ii) If $|\mathcal{Z}| < \mathcal{Z}_{th}$, the potential $U(\varphi)$ becomes a monotonically decreasing function [blue and dashed lines in Fig. 2(a)]. In configuration (i), the phase particle cannot leave the region of its initial location. Hence, it moves towards a local minimum. As this motion affects the direction of the precession axis $\mathbf{N}(t)$, the whole system starts to display damped oscillations because energy is dissipated via the resistance. If the bias current is sufficiently small $I_{DC} \ll I_c$, the phase particle and the Majorana qubit eventually reach fixed points φ_0 and $\mathbf{R}_0$ as

$t \to \infty$ and stop moving. Therefore, after a transient time, the average voltage drop vanishes, $V = 0$, and the ground state carries the supercurrent I_{DC} without resistance. We provide analytic solutions of the fixed points and numerical results of $\varphi(t)$ and $\mathbf{R}(t)$ in the SM [44].

As a physical consequence of finite interedge coupling E_x, we find that finite voltage develops as the bias current increases but still fulfills $I_{DC} < I_c$. A finite value of E_x stimulates the Majorana qubit to evolve from the state $|0_{12}0_{34}\rangle$ into a superposition of the opposite current-carrying states $|0_{12}0_{34}\rangle$ and $|1_{12}1_{34}\rangle$, corresponding to $|\mathcal{Z}| < 1$. Hence, the configuration (ii) of the washboard potential $|\mathcal{Z}| < \mathcal{Z}_{th} = I_{DC}/I_c$ can occur and the phase particle can roll down. A sustained onset of this mechanism leads to a finite V and therefore to a reduction of the critical current I_c^* of the junction. The analytical computation of I_c^* confirms the existence of this effect. In particular, by computing the maximal current carried by the ground state of the system, we obtain

$$I_c^* = \sqrt{I_c^2 + \left(\frac{eE_x}{\hbar}\right)^2} - \frac{eE_x}{\hbar} \leqslant I_c \tag{5}$$

which is indeed lowered by a finite interedge coupling E_x [44]. In Fig. 2(b), we show the agreement between Eq. (5) (white dashed line) and the numerical computation of V, which features finite values even for I_{DC} well below I_c. As the lowering of the critical current traces back to the fusion properties of the four MBSs hosted by the TJJ, it represents an important insight of our work.

DC Shapiro steps. Interestingly, an in-depth analysis of the average voltage V in the regime $I_{DC} \geqslant I_c^*$ reveals a more striking effect: V features sequential sudden steps as the DC current increases. We provide numerical computations of V in Figs. 2(b) and 3(a) with realistic experimental parameters [36]. The voltage is averaged over a time period $2 \times 10^3 \tau_r \sim 160$ ns. In Fig. 3(a), where we consider a ratio $E_x/E_M = 0.67$, more than four sequential jumps are visible. These jumps are the DC Shapiro steps.

To understand their physical origin, we analyze further the mechanism responsible for the rolling of the phase particle down the washboard potential. The key observation is that, for $I_{DC} > I_c^*$, the oscillations of $\mathcal{Z}(t)$ make the washboard potential keep alternating between configurations (i) and (ii) (described above). Hence, it can still develop local minima, which temporarily trap the phase particle. The motion of the phase particle thus alternates between oscillations around one local minimum and the rolling from a region R_j down to the next region R_{j+1}. The integer number of oscillations within a single region decreases as the average slope of the washboard potential I_{DC} is increased. When this number changes by one, it abruptly modifies the dwelling time Ω^{-1} of the phase particle within a single region, which causes a sudden jump of the average voltage $V = h\Omega/(2e)$. We observe that, in between the steps, the voltage does not feature flat plateaus, as the frequency Ω continuously increases with I_{DC}, even for a fixed number of oscillations. In the SM [44], we provide short movies which display the time evolution of the system.

Supported by the numerical analysis of the trajectories followed by $\mathbf{R}(t)$ [see Figs. 3(b)–3(d)], we identify the following
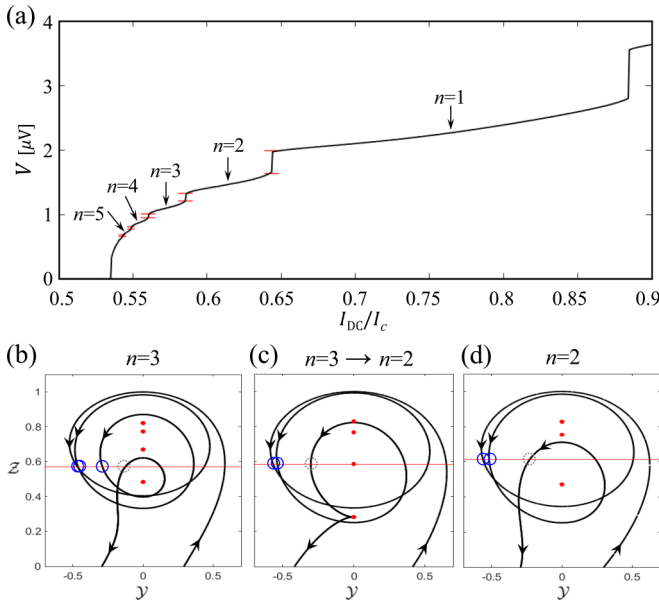
FIG. 3. (a) A current-voltage curve for $E_x/E_M = 0.67$. The number n of recapturing the phase particle is indicated and the analytically estimated size of jumps is shown with horizontal lines (red). (b)–(d) The trajectories of $[\mathcal{Y}(t), \mathcal{Z}(t)]$ are displayed for various n. The Majorana qubit rotates around **N** with the counterclockwise direction (black arrows). At $t = 0, T, 2T, \ldots$, solid circles (red) indicate the normalized precession axis $\hat{N} = \mathbf{N}/||\mathbf{N}||$, which approaches to $\mathcal{Z} = 0$ monotonically. The horizontal red lines depict the threshold $\mathcal{Z} = \mathcal{Z}_{th}$. When the trajectory intercepts the red line with $\ddot{\mathcal{Z}} = \epsilon_x \dot{\mathcal{Y}} > 0$ (blue circles), the phase particle is recaptured. Contrarily, when the condition $\ddot{\mathcal{Z}} = \epsilon_x \dot{\mathcal{Y}} < 0$ is met (dotted circles), $\mathcal{Z}$ keeps on decreasing and flips its sign, allowing the phase particle to roll down. The voltage V jumps exactly when the number of recapturing n decreases [panel (c)]. We use the same parameters as in Fig. 2.

criteria to understand whether the phase particle is captured at a local minimum or if it rolls down to the next local minimum. For concreteness, we display the passage between regions R_1 and R_2 in Fig. 2(a). When $\mathcal{Z}(t) > \mathcal{Z}_{th}$, region R_1 features a local minimum, which can trap the phase particle. Once the system dynamics lowers $\mathcal{Z}(t)$ to $\mathcal{Z}(t) = \mathcal{Z}_{th}$, the subsequent evolution of the system depends on the sign of the second derivative $\ddot{\mathcal{Z}} = \epsilon_x \mathcal{Y}$. If $\ddot{\mathcal{Z}}$ is positive, $\mathcal{Z}(t)$ rapidly increases back above the threshold and the phase particle is recaptured by the local minimum in R_1. By contrast, if $\ddot{\mathcal{Z}} < 0$, $\mathcal{Z}(t)$ keeps on diminishing and eventually flips sign as the phase particle enters the next region R_2. The system then follows an analogous evolution, since Eqs. (3) and (4) are symmetric under $\mathcal{Y} \to -\mathcal{Y}$, $\mathcal{Z} \to -\mathcal{Z}$, and $\varphi \to \varphi + 2\pi$.

As anticipated before, the steps in the average voltage V are associated with changes in the number n of subsequent recapturing processes [see Figs. 3(b)–3(d). In Fig. 3(b), the

trajectories of $\mathbf{R}(t)$ show that the phase particle is recaptured $n = 3$ times before it can roll down to the next region and $\mathcal{Z}$ can flip sign. In Fig. 3(c), where we increase the bias current to exactly match the DC Shapiro step in Fig. 3(a), we observe a vanishing second derivative $\ddot{\mathcal{Z}} = \epsilon_x \mathcal{Y}$ when $\mathcal{Z}$ lowers to $\mathcal{Z}_{th}$ for the third time. In Fig. 3(d), with a higher bias current I_{DC}, the phase particle is recaptured two times ($n = 2$) before rolling down to the next region. With increasing I_{DC}, two more steps appear when $n = 2 \to 1$ and $n = 1 \to 0$.

We give an estimation of the height of the DC Shapiro steps. To this end, close to the jumps, we roughly approximate the dwelling time within a single region as $\Omega_n^{-1} \sim n\mathcal{T}$, where $\mathcal{T}$ is the precession period of $\mathbf{R}(t)$. We estimate the latter as $1/\mathcal{T} \sim (E_x^2 E_M^2 + E_x^4)^{1/4}/(\pi \hbar)$ by assuming an almost constant $\cos(\varphi) \sim -(I_c^*/I_c)^2$. We can therefore compute the size of the jumps as $\Delta V = (\Omega_n - \Omega_{n+1})h/(2e)$, which agrees with the numerical result in Fig. 3(a). Hence, observations of the size of steps provide a way to estimate the Rabi frequency $1/\mathcal{T}$ of the Majorana qubit by assigning n to the steps and using the formula for ΔV written above. Notice that ΔV vanishes when $E_x = 0$.

Robustness. Our findings are robust against a finite capacitance of the junction [44]. Moreover, we analyze the influence of an additional 2π-periodic supercurrent, which could be larger in magnitude up to three times of the 4π-periodic supercurrent in Eq. (3). Since the alternating configurations of the washboard potential remain qualitatively similar, DC Shapiro steps are preserved [44].

Furthermore, we explicitly check that the DC Shapiro steps are robust against decoherence, when the timescales for the decoherence are much longer than the period of the Rabi oscillation $\mathcal{T}$. The trajectories of the Majorana qubit, which lead to DC Shapiro steps [see Fig. 3(b)], form the limit cycles [53], to which the nonlinear dynamics of the system eventually converges. Hence, the dynamics of the Majorana qubit and DC Shapiro steps are intact if decoherence happens at larger timescales. We show the robustness of DC Shapiro steps against decoherence by considering parity flipping by nearby impurities and quasiparticle poisoning by thermal environments [44].

Summary. We have investigated a novel Josephson effect of a TJJ hosting a Majorana qubit. We have predicted a lowering of the critical current and the emergence of DC Shapiro steps. Notably, the detection of DC Shapiro steps is measurable with the same experimental techniques as the ones used to observe the AC Shapiro steps in TJJs [35,36,54]. Therefore, we are confident that our proposal is feasible.

[1] A. Y. Kitaev, Unpaired Majorana fermions in quantum wires, Phys. Usp. **44**, 131 (2001).

[2] C. Nayak, S. Simon, A. H. Stern, M. Freedman, and S. Das Sarma, "Non-Abelian anyons and topological quantum computation," Rev. Mod. Phys. **80**, 1083 (2008).

[3] J. Alicea, Y. Oreg, G. Refael, F. von Oppen, and M. P. A. Fisher, Non-Abelian statistics and topological quantum information processing in 1D wire networks, Nat. Phys. **7**, 412 (2011).

[4] M. Leijnse and K. Flensberg, Introduction to topological superconductivity and Majorana fermions, Semicond. Sci. Technol. **27**, 124003 (2012).

[5] D. Aasen, M. Hell, R. V. Mishmash, A. Higginbotham, J. Danon, M. Leijnse, T. S. Jespersen, J. A. Folk, C. M. Marcus, K. Flensberg *et al.*, Milestones Toward Majorana-Based Quantum Computing, Phys. Rev. X **6**, 031016 (2016).

[6] D. A. Ivanov, Non-Abelian Statistics of Half-Quantum Vortices in *p*-Wave Superconductors, Phys. Rev. Lett. **86**, 268 (2001).

[7] S. Bravyi, Universal quantum computation with the $\nu = 5/2$ fractional quantum Hall state, Phys. Rev. A **73**, 042313 (2006).

[8] E. C. Rowell and Z. Wang, Degeneracy and non-Abelian statistics, Phys. Rev. A **93**, 030102 (2016).

[9] Y. Oreg, G. Refael, and F. von Oppen, Helical Liquids and Majorana Bound States in Quantum Wires, Phys. Rev. Lett. **105**, 177002 (2010).

[10] R. M. Lutchyn, J. D. Sau, and S. Das Sarma, Majorana Fermions and a Topological Phase Transition in Semiconductor-Superconductor Heterostructures, Phys. Rev. Lett. **105**, 077001 (2010).

[11] V. Mourik, K. Zuo, S. M. Frolov, S. R. Plissard, E. P. A. M. Bakkers, and L. P. Kouwenhoven, Signatures of Majorana fermions in hybrid superconductor-semiconductor nanowire devices, Science **336**, 1003 (2012).

[12] S. M. Albrecht, A. P. Higginbotham, M. Madsen, F. Kuemmeth, T. S. Jespersen, J. Nygård, P. Krogstrup, and C. M. Marcus, Exponential protection of zero modes in Majorana islands, Nature (London) **531**, 206 (2016).

[13] M. T. Deng, S. Vaitiekenas, E. B. Hansen, J. Danon, M. Leijnse, K. Flensberg, J. Nygård, P. Krogstrup, and C. M. Marcus, Majorana bound state in a coupled quantum-dot hybrid-nanowire system, Science **354**, 1557 (2016).

[14] Ö. Gül, H. Zhang, J. D. S. Bommer, M. W. A. de Moor, D. Car, S. R. Plissard, E. P. A. M. Bakkers, A. Geresdi, K. Watanabe, T. Taniguchi, and L. P. Kouwenhoven, Ballistic Majorana nanowire devices, Nat. Nanotechnol. **13**, 192 (2018).

[15] Z. Yan, F. Song, and Z. Wang, Majorana Corner Modes in A High-Temperature Platform, Phys. Rev. Lett. **121**, 096803 (2018).

[16] Q. Wang, C. Liu, Y. Lu, and F. Zhang, High-Temperature Majorana Corner States, Phys. Rev. Lett. **121**, 186801 (2018).

[17] X. Zhu, Tunable Majorana corner states in a two-dimensional second-order topological superconductor induced by magnetic fields, Phys. Rev. B **97**, 205134 (2018).

[18] M. Geier, L. Trifunovic, M. Hoskam, and P. W. Brouwer, Second-order topological insulators and superconductors with an order-two crystalline symmetry, Phys. Rev. B **97**, 205135 (2018).

[19] E. Khalaf, Higher-order topological insulators and superconductors protected by inversion symmetry, Phys. Rev. B **97**, 205136 (2018).

[20] C.-H. Hsu, P. Stano, J. Klinovaja, and D. Loss, Majorana Kramers Pairs in Higher-Order Topological Insulators, Phys. Rev. Lett. **121**, 196801 (2018).

[21] R.-X. Zhang, W. S. Cole, and S. Das Sarma, Helical Hinge Majorana Modes in Iron-Based Superconductors, Phys. Rev. Lett. **122**, 187001 (2019).

[22] S.-B. Zhang, W. B. Rui, A. Calzona, S.-J. Choi, A. P. Schnyder, and B. Trauzettel, Topological and holonomic quantum computation based on second-order topological superconductors, arXiv:2002.05741.

[23] S.-B. Zhang, A. Calzona, and B. Trauzettel, All-electrically tunable networks of Majorana bound states, Phys. Rev. B **102**, 100503 (2020).

[24] L. Fu and C. L. Kane, Superconducting Proximity Effect and Majorana Fermions at the Surface of a Topological Insulator, Phys. Rev. Lett. **100**, 096407 (2008).

[25] F. Pientka, A. Keselman, E. Berg, A. Yacoby, A. Stern, and B. I. Halperin, Topological Superconductivity in a Planar Josephson Junction, Phys. Rev. X **7**, 021032 (2017).

[26] S.-J. Choi and H.-S. Sim, "Non-abelian evolution of a majorana train in a single josephson junction," arXiv:1808.08714.

[27] S. Guiducci, M. Carrega, F. Taddei, G. Biasiol, H. Courtois, F. Beltram, and S. Heun, Full electrostatic control of quantum interference in an extended trenched Josephson junction, Phys. Rev. B **99**, 235419 (2019).

[28] A. Fornieri, A. M. Whiticar, F. Setiawan, E. Portolés, A. C. C. Drachmann, A. Keselman, S. Gronin, C. Thomas, T. Wang, R. Kallaher *et al.*, Evidence of topological superconductivity in planar Josephson junctions, Nature (London) **569**, 89 (2019).

[29] A. Calzona and B. Trauzettel, Moving Majorana bound states between distinct helical edges across a quantum point contact, Phys. Rev. Res. **1**, 033212 (2019).

[30] L. Fu and C. L. Kane, Josephson current and noise at a superconductor/quantum-spin-Hall-insulator/superconductor junction, Phys. Rev. B **79**, 161408(R) (2009).

[31] D. M. Badiane, M. Houzet, and J. S. Meyer, Nonequilibrium Josephson Effect through Helical Edge States, Phys. Rev. Lett. **107**, 177002 (2011).

[32] L. Jiang, D. Pekker, J. Alicea, G. Refael, Y. Oreg, and F. von Oppen, Unconventional Josephson Signatures of Majorana Bound States, Phys. Rev. Lett. **107**, 236401 (2011).

[33] P. San-Jose, E. Prada, and R. Aguado, ac Josephson Effect in Finite-Length Nanowire Junctions with Majorana Modes, Phys. Rev. Lett. **108**, 257001 (2012).

[34] L. P. Rokhinson, X. Liu, and J. K. Furdyna, The fractional ac Josephson effect in a semiconductor-superconductor nanowire as a signature of Majorana particles, Nat. Phys. **8**, 795 (2012).

[35] J. Wiedenmann, E. Bocquillon, R. S. Deacon, S. Hartinger, O. Herrmann, T. M. Klapwijk, L. Maier, C. Ames, C. Brüne, C. Gould *et al.*, 4π-periodic Josephson supercurrent in HgTe-based topological Josephson junctions, Nat. Commun. **7**, 10303 (2016).

[36] E. Bocquillon, R. S. Deacon, J. Wiedenmann, P. Leubner, T. M. Klapwijk, C. Brüne, K. Ishibashi, H. Buhmann, and L. W. Molenkamp, Gapless Andreev bound states in the quantum spin Hall insulator HgTe, Nat. Nanotechnol. **12**, 137 (2017).

[37] E. Bocquillon, J. Wiedenmann, R. S. Deacon, T. M. Klapwijk, H. Buhmann, and L. W. Molenkamp, *Topological Matter* (Springer International Publishing, Basel, 2018).

[38] D. Laroche, D. Bouman, D. J. van Woerkom, A. Proutski, C. Murthy, D. I. Pikulin, C. Nayak, R. J. J. van Gulik, J. Nygård, P. Krogstrup *et al.*, Observation of the 4π-periodic Josephson effect in indium arsenide nanowires, Nat. Commun. **10**, 245 (2019).

[39] J. Wang, Controllable Majorana fermions on domain walls of a magnetic topological insulator, Phys. Rev. B **98**, 024519 (2018).

[40] J.-J. Feng, Z. Huang, Z. Wang, and Q. Niu, Hysteresis from nonlinear dynamics of Majorana modes in topological Josephson junctions, Phys. Rev. B **98**, 134515 (2018).

[41] J.-J. Feng, Z. Huang, Z. Wang, and Q. Niu, Josephson radiation from nonlinear dynamics of Majorana zero modes, Phys. Rev. B **101**, 180504(R) (2020).

[42] S. Shapiro, Josephson Currents in Superconducting Tunneling: The Effect of Microwaves and Other Observations, Phys. Rev. Lett. **11**, 80 (1963).

[43] M. Tinkham, *Introduction to superconductivity* (McGraw-Hill, New York, 1996).

[44] See the Supplemental Material at http://link.aps.org/supplemental/10.1103/PhysRevB.102.140501, which includes Refs. [45–51], for the derivation of the interedge coupling E_x, the fixed points of φ_0 and $\mathcal{Z}_0$, an alternative derivation of I_c^*, numerical results of the Josephson effect when $I_{DC} \ll I_c^*$, effects of a finite capacitance and a 2π-periodic contribution to the supercurrent, and the effect of decoherence on DC Shapiro steps.

[45] Z.-X. Li, A. Vaezi, C. B. Mendl, and H. Yao, Numerical observation of emergent spacetime super-symmetry at quantum criticality, Sci. Adv. **4**, eaau1463 (2018).

[46] A. P. Higginbotham, S. M. Albrecht, G. Kirsanskas, W. Chang, F. Kuemmeth, P. Krogstrup, T. S. Jespersen, J. Nygård, K. Flensberg, and C. M. Marcus, Nat. Phys. **11**, 1017 (2015).

[47] J. C. Budich, S. Walter, and B. Trauzettel, Failure of protection of Majorana based qubits against decoherence, Phys. Rev. B **85**, 121405(R) (2012).

[48] D. Rainis and D. Loss, Majorana qubit decoherence by quasi-particle poisoning, Phys. Rev. B **85**, 174533 (2012).

[49] P. J. de Visser, J. J. A. Baselmans, P. Diener, S. J. C. Yates, A. Endo, and T. M. Klapwijk, Parity Lifetime of Bound States in a Proximitized Semiconductor Nanowire, Phys. Rev. Lett. **106**, 167004 (2011).

[50] S. M. Albrecht, E. B. Hansen, A. P. Higginbotham, F. Kuemmeth, T. S. Jespersen, J. Nygård, P. Krogstrup, J. Danon, K. Flensberg, and C. M. Marcus, Transport Signatures of Quasi-particle Poisoning in a Majorana Island, Phys. Rev. Lett. **118**, 137701 (2017).

[51] M. A. Nielsen and I. L. Chuang, *Quantum Computation and Quantum Information* (Cambridge University Press, Cambridge, UK, 2010).

[52] F. Crépin and B. Trauzettel, Parity Measurement in Topological Josephson Junctions, Phys. Rev. Lett. **112**, 077002 (2014).

[53] The trajectory of the Majorana qubit satisfies the conditions for the limit cycle stated in the following papers: S. M. Shahruz, Generation of self-pulsation in passively Q-switched lasers, Physica D **142**, 291 (2000); S. M. Shahruz and D. A. Kalkin, Limit cycle behavior in three or higher-dimensional non-linear systems: The Lotka-Volterra example, J. Sound Vib. **246**, 379 (2001).

[54] S. Hart, H. Ren, T. Wagner, P. Leubner, M. Mühlbauer, C. Brüne, H. Buhmann, L. W. Molenkamp, and A. Yacoby, Induced superconductivity in the quantum spin Hall edge, Nat. Phys. **10**, 638 (2014).